Starch biocomposites preparation by incorporating organosolv lignins from potato crop residues

Shiva Zolfaghari[a], Ali Soltaninejad[a], Oseweuba Valentine Okoro[b], Amin Shavandi[b], Joeri F.M. Denayer[c], Morteza Sadeghi[a,d], Keikhosro Karimi[c*]

[a] Department of Chemical Engineering, Isfahan University of Technology, Isfahan, 84156-83111, Iran

[b] Université libre de Bruxelles (ULB), École polytechnique de Bruxelles, 3BIO-BioMatter, Avenue F.D. Roosevelt, 50 - CP 165/61, 1050 Brussels, Belgium

[c] Department of Chemical Engineering, Vrije Universiteit Brussel, 1050 Brussels, Belgium

[d] School of Engineering, Faculty of Science and Engineering, Macquarie University, Sydney, NSW 2109, Australia

Corresponding author:

E-mail address: Keikhosro.Karimi@vub.be

Tel :+32 (0) 495781049

Fax: +32 (0) 26293512

Symbols abbreviated

AIL = Acid insoluble lignin; ASL = Acid soluble lignin; ATR-FTIR = Attenuated total reflection-Fourier transform infrared; DTG = Derivative Thermogravimetry; FE-SEM = Field emission scanning electron microscope; OPL = Organosolv lignin from potato crop residues; PCR = Potato crop residues; rpm = revolutions per minute; TGA = Thermogravimetric analysis; UV–Vis = Ultraviolet–visible spectroscopy; WVTR = Water vapor transmission rate; XRD = X-ray diffraction

Abstract

Plastic wastes accumulated due to food packaging pose environmental threats. This study proposes biopolymeric films containing lignins extracted from potato crop residues (PCR) through organosolv treatment as a green alternative to non-degradable food packaging. The isolation process yielded 43.9 wt.% lignins with a recovery rate of 73.5 wt.% achieved under optimum conditions at 180 °C with 50% v/v ethanol. The extracted lignins were then incorporated into a starch matrix to create biocomposite films. ATR-FTIR analysis confirmed interactions between the starch matrix and extracted lignins, and XRD analysis showed the amorphous structure of lignins, reducing film crystallinity. The addition of 1 wt.% of extracted lignins resulted in a 87% reduction in oxygen permeability, a 25% increase in the thermal stability of the film, and a 78% enhancement in antioxidant. Furthermore, introducing 3 wt.% lignins led to the lowest water vapor transmission rate, measuring 9.3×10^{-7} kg/s·m². Morphological studies of the films demonstrated a homogeneous and continuous structure on both the surface and cross-sectional areas when the lignins content was below 7 wt.%. These findings highlight the potential of using organosolv lignins derived from potato crop residues as a promising additive for developing eco-friendly films designed for sustainable food packaging.

Keywords: Biopolymer; Food packaging; Crop waste valorization

1. Introduction

In recent years, the increasing emphasis on responsible consumption and production has driven researchers to investigate more environmentally friendly options to replace fossil-based polymers [1]. This is due, in part, to the fact that current plastic waste recycling methods have not resulted in a significant reduction in the amount of plastic waste being disposed of in the environment, landfills, or through incineration. Indeed, current trends indicate that the mass of plastic waste generated is projected to reach 150 million tons by the year 2050 [2], further exacerbating the negative consequences associated with existing waste management approaches. These challenges include groundwater pollution caused by the leaching of plastic waste and the release of harmful chemicals like dioxins, furans, and polychlorinated biphenyls into the environment during incineration [2]. To address these waste management issues, the substitution of traditional fossil-based polymers with biobased alternatives has emerged as a viable solution [3]. Biobased polymers, or biopolymers, have gained significant attention for diverse applications, including the development of food packaging materials [4].

Among biopolymers, starch stands out as a promising replacement for non-degradable polymers due to its biodegradability, sustainability, widespread availability, and cost-effectiveness [5]. Starch, a polysaccharide biopolymer, is primarily found in plants [6], such as maize, cassava, wheat, rice, and potatoes, where it serves as a reserve of sugar molecules [7]. Despite its favorable film-forming properties, starch-based films are characterized by poor resistance to moisture due to their hydrophilic nature and limited mechanical strength [8, 9].

To enhance the properties of starch-based films, various modification techniques have been explored. These methods range from chemical modifications to the incorporation of different polymers, compounds, and fillers into starch matrices [10]. The incorporation of natural fillers is

of particular interest due to their affordability and biodegradability, with lignins being identified as a promising natural polymer to be used alongside starch in film production [11]. Lignins, the second most abundant natural polymer after cellulose, are present in the cell walls of lignocellulosic materials and serve as binding agents [12-15]. Lignins consist of chemical units that contribute to hydrophobicity, UV absorption, and antioxidant properties when used as a filler in composites [16]. Comprising aliphatic and aromatic compounds, lignins are biosynthesized from components such as p-coumaryl alcohol, coniferyl alcohol, and sinapyl alcohol [17]. Their structure is influenced by botanical source and extraction methods [18]. In alignment with the principles of a circular economy [19], lignins sourced from highly polluting potato crop residues (PCR-lignins) could be a valuable natural filler, as up to 46 million tons of potato crop residues (PCR) are generated globally each year [20]. Utilizing them can help mitigate associated pollution challenges [21]. In this study, the organosolv process was employed to recover lignins from PCR. In comparison to other lignin extraction methods such as kraft, sulfite, and soda processes [22, 23], the organosolv process facilitates the efficient recovery of high-purity, sulfur-free lignin [24]. Additionally, the organosolv treatment can be integrated into other processes through solvent selection and can be made more economically viable through solvent recovery [25]. Importantly, a literature review indicates that the extraction of lignins from potato crop residues and their subsequent use to reinforce starch-based biocomposites has yet to be explored.

The objective of the present study is to utilize organosolv lignins from potato crop residues to produce innovative biodegradable biocomposites for food packaging. The impact of lignin content on the properties of the prepared films was investigated through various analyses, and the results are discussed in detail. The chemical composition of starch films and lignin particles incorporated into the starch matrix was determined using ATR-FTIR. The influence of lignins on

the starch matrix was further evaluated through mechanical testing, X-ray diffraction, FE-SEM, TGA, UV-Vis spectrophotometry, oxygen permeation testing, water vapor transmission rate measurement, water swelling analysis, and antioxidant assays.

2. Materials and methods

2.1. Materials

Food-grade wheat starch was purchased from Chavil Food Industries, Iran, and its structural properties were previously investigated in our research [26]. The chemical characteristics of this component, provided by the producer, are detailed in supplementary data Table S1. Deionized water (conductivity < 1 μS/cm) was employed to prepare aqueous-based mixtures. Oxygen (ACS Grade, ~100% purity) was sourced from Ardestan Gas Co., Iran, and used to measure the gas permeability of the biocomposite film.

2.2. Raw materials and preparation of the potato crop residues

The potato crop residues used in this study were collected during the harvest season of October 2019 from a cultivation field located in Fereydun Shar, Isfahan, Iran. The geographical location of the farm is 32° 94′ 01″ N, 50° 12′ 40″ E. These residues primarily consisted of stalks and leaves, which were separated from other parts of the plants. Subsequently, the residues were ground and sieved using Endecott sieves with mesh sizes of 20 and 80 to achieve particle sizes ranging from 0.177 mm to 0.833 mm. Following this, potato crop residues were dried in a convection oven at 105 °C to achieve a constant weight, following the method provided by Sluiter et al. [29]. The dried residues were then stored in plastic bags at room temperature for future use.

2.3. Organosolv lignin extraction and characterization

Organosolv treatment was conducted using a stainless steel reactor with a capacity of 500 mL, immersed in an oil bath set to the desired temperature at a heating rate of 3°C per minute. The reactor was equipped with temperature and pressure controllers and monitors. Treatments were carried out at temperatures of 120°C, 150°C, and 180°C, with ethanol solvent concentrations of 50% v/v and 75% v/v [27].

For the organosolv process, a mixture of 20 g of PCR was combined with 180 g of an ethanol-water solution and loaded into the reactor. The organosolv process was maintained for 1 hour [28]. Following completion of the organosolv process, the reactor was cooled to room temperature, and a filtration operation was performed to recover the solid fraction (treated PCR) from the filtrate. Subsequently, 300 mL of ethanol (50% v/v) was utilized to wash the treated PCR at 60°C, effectively removing residual lignins from its surface. The washed-treated PCR was then collected, and the liquid phase was retained for lignin precipitation. The two-stage lignin precipitation process began with centrifuging the obtained liquor at 4500 rpm for 5 minutes to separate solids. Next, the liquid phase was mixed with three volumes of water and subjected to another round of centrifugation at 4500 rpm for 5 minutes, resulting in the collection of the precipitated lignin as the second-stage lignin. This combination of the first and second stages of lignin precipitation was used for film preparation as PCR-lignins, and any remaining liquid was stored in the refrigerator at 4°C [25].

The precipitated lignins were separated, washed through centrifugation (4000 rpm for 15 minutes), and then subjected to drying. Initially, they were dried in an oven at 40°C for 48 hours, followed by additional drying in a vacuum oven at 30°C for 24 hours to ensure complete moisture removal. The dried lignins were stored in moisture-free, airtight bags at room

temperature until use. The treated PCR was also dried for 48 hours at 40°C in an oven to reach a constant mass. Material recovery was calculated using Eq. (1):

$$\text{Material recovery} = \frac{\text{treated PCR (g)}}{\text{Initial substrate (g)}} \times 100 \quad (1)$$

The composition of the samples from treated and raw PCR, as well as the extracted lignins, was determined following the method recommended by the National Renewable Energy Laboratory (NREL) [29]. In brief, a two-step acid-based hydrolysis using H_2SO_4 was carried out to solubilize the acid-soluble lignin (ASL) and carbohydrates in the samples. Initially, the samples were mixed with 3 mL of sulfuric acid (72% w/w) and incubated for 1 hour at 30 °C. Subsequently, 84 mL of distilled water was added to dilute the acid concentration to 4%. The samples were then autoclaved at 121 °C for 1 hour, and the liquid phase was separated from the solid residues using vacuum filtration. The resulting filtrate was used to determine the ASL and carbohydrate content of the samples.

The monomeric polymers produced from the acid-based hydrolysis of carbohydrate polymers were quantified using high-performance liquid chromatography (HPLC). The ASL fraction in the samples was determined using UV spectroscopy, while Klason lignin was measured through gravimetric analysis of the remaining solid residues. Xylan and lignin removal, lignin yield and recovery, and lignin purity were calculated using Eqs. (2) to (6), respectively.

$$\text{Xylan removal (\%)} = 100 - \frac{\text{Material recovery of treatment (\%)} \times \text{Xylan content of treated PCR (\%)}}{\text{Xylan content of initial substrate (\%)}} \quad (2)$$

$$\text{Lignin removal (\%)} = 100 - \frac{\text{Material recovery of treatment (\%)} \times \text{Lignin content of treated PCR (\%)}}{\text{Lignin content of initial substrate (\%)}} \quad (3)$$

$$\text{Lignin yield (\%)} = \frac{\text{Total mass of extracted PCR-lignin}}{\text{Lignin content of initial PCR}} \times 100 \quad (4)$$

$$\text{Lignin recovery (\%)} = \frac{\text{Total mass of extracted PCR-lignin}}{\text{Lignin content of initial PCR-Lignin content of treated PCR}} \times 100 \quad (5)$$

$$\text{Lignin purity (\%)} = \frac{\text{Lignin content of lignin-rich fraction}}{\text{Lignin-rich fraction total mass}} \times 100 \quad (6)$$

2.4. Preparation of films

The composite films were fabricated using the solution-casting method, with OPL mass ratios of 1%, 3%, 7%, 9%, and 11% being varied relative to the starch powder. These films were designated as OPL-1%, OPL-3%, OPL-5%, OPL-7%, OPL-9%, and OPL-11%, respectively, as indicated in Eq. (7):

$$\text{OPL loading (wt.\%)} = \frac{\text{mass of OPL (g)}}{\text{mass of OPL (g)+mass of Starch (g)}} \times 100 \quad (7)$$

In this regard, a 6 wt.% starch suspension was prepared by adding starch powder to deionized water, followed by agitation through sonication for 1 hour. Subsequently, the starch suspension mixture was stirred and heated for 30 minutes at 90°C, and glycerol was added as a plasticizer (40% w/w of the starch powder mass). The resulting gelatinized starch was stirred and heated at 90°C for an additional 30 minutes. Then, the OPL was introduced into an ethanol:water solution (70:30, v:v) to achieve a 1 wt.% lignin solution, which was heated at 60°C for 1 hour. Both the gelatinized starch and OPL solution were cooled to 50°C. The OPL solution was then slowly added drop by drop to the gelatinized starch, and the resulting mixture was stirred for 1 hour at 50°C. It was subsequently degassed through sonication and cooling to 40°C. Casting of the mixture was performed using a plexiglass Petri dish, pre-dried in an oven at 36°C for 24 hours,

and then dried for an additional 24 hours in a vacuum oven at 25°C. A film composed solely of starch was also prepared in a similar manner and served as the control. The prepared films were stored in a moisture-free environment at room temperature, within desiccators, prior to characterization. Film thickness was measured using a handheld micrometer in 10 random replicates, and the mean values were used for calculations.

2.5. Film and organosolv-treated sample characterization

Attenuated total reflection-Fourier transform infrared (ATR-FTIR) analysis (Bruker Tensor 27, Bruker, Germany) was conducted over wavenumbers ranging from 400 to 4000 cm^{-1} to examine the chemical structure of the films and potential interactions between starch and the extracted lignins (PCR-lignins). X-ray diffraction (XRD) patterns of lignins powder and films were obtained using a PMD Philips X-pert instrument (Philips, Netherlands) with Cu Kα radiation, scanning at a rate of 5° min-1 within the range of 10°–60°. The surface morphology and cross-sectional area of the films, as well as the morphology of PCR-lignins, were analyzed using a field emission scanning electron microscope (FE-SEM, Mira 3-XMU, TESCAN Ltd., Czech Republic) operating at 5 kV. Furthermore, morphological analysis of untreated and treated samples subjected to organosolv treatment was performed using SEM (SEM, Zeiss, Germany) to investigate structural changes induced by organosolv treatment.

Thermal stability assessments of lignins and the prepared films were carried out using thermogravimetric analysis (TGA), involving heating from 25°C to 750°C (heating rate = 10°C/min) under a nitrogen atmosphere. TGA measurements were performed using a METTLER TOLEDO TGA instrument (Switzerland). Key temperatures for analysis included T5, T30, and T50, representing the temperatures corresponding to 5%, 30%, and 50% mass loss, respectively.

Additionally, Tonset, indicating the temperature at the onset of sample mass loss, and Tmax, representing the peak temperature of the derivative mass curve, were determined.

Mechanical testing of the films followed the ASTM D882 standard [30]. A Zwick Roell tensile tester from Germany, operating at a crosshead speed of 10 mm/min, was employed for this purpose. Specimens were cut into strips, and the mean result of five replicates was subsequently reported. A UV-visible spectrophotometer (UV-1601, Rayleigh, Beijing, China) was used to capture the transmission spectrum of the films in the range of 200 to 800 nm. Opacity values of the fabricated films were calculated as follows [31]:

$$\text{Opacity} = Abs_{600}/X \quad (8)$$

where Abs_{600} and X represent the absorbance at 600 nm and film thickness (mm), respectively. This procedure was repeated three times for each sample.

The antioxidant capacity of the prepared films was investigated using the DPPH (2,2-diphenyl-1-picrylhydrazyl) free radical scavenging assay as explained by Mao et al. [32]. Initially, samples were soaked in 5 mL of methanol and shaken for 3 hours at 25 °C. Afterward, a 0.2 mL solution containing 1 mmol of DPPH in 1 L of methanol was mixed with 1 mL of film extract obtained from the previous step. This mixture was then placed in a dark incubator for 30 minutes. An equal volume of methanolic DPPH solution was considered as the control sample. The absorbance of the prepared samples was recorded at 517 nm, and the antioxidant activity was calculated as follows [32]:

$$\text{Antioxidant activity (\%)} = \frac{A_c - A_s}{A_c} \times 100 \quad (9)$$

where A_s is the absorbance of blended samples, and A_c is the absorbance of control.

222 2.5.1. Gas permeability measurement

223 The oxygen permeability of the prepared films was measured following the ASTM
224 Standard Method D1434 [33] (variable pressure and constant volume) at 25 °C and 1 bar, using a
225 cell lab (manifold), and calculated as follows;

226 $$P = \frac{dp}{dt} \times \frac{273.15 \times 13.7 \times 10^{10} \times L}{76 \times A \times T \times P_0} \quad (10)$$

227 where P represents the oxygen permeability (1 Barrer = 1×10^{10} cm^3 (STP) cm/cm^2.s.Hg), dp/dt
228 is the rate of pressure increase obtained by drawing the trendline on the pressure-time graph
229 (mbar/s). Additionally, L, A, T, and $P_\circ$ represent the effective thickness (cm), effective area of
230 the film (cm^2), operating temperature (K), and the operating pressure applied in the high-pressure
231 chamber (mbar), respectively. Oxygen permeation was performed three times for each sample
232 [26].

233 2.5.2. Water vapor transmission rate (WVTR) and water swelling

234 The capacity of the films to act as a barrier was evaluated based on the ASTM E-96-96
235 method [34]. Briefly, the samples were initially conditioned at 25 °C and 40% relative humidity
236 (RH) until a constant mass was attained. These films were introduced to test containers
237 containing 50 g of distilled water. The test containers were maintained at 25 °C and 40% RH and
238 weighed every 12 h for 14 days, with the loss in the mass of each container subsequently
239 determined. The WVTR was calculated as follows:

240 $$WVT = \Delta m / (\Delta t \times A) \quad (11)$$

241 where Δm denotes the mass loss of water from the container, Δt is the duration of the experiment,
242 and A is the exposed film surface area to water vapor.

The water swelling capacity of the films was analyzed following the procedure outlined in our previous study [26], and the swelling index was calculated using Eq. (12).

$$\text{Water swelling (\%)} = \frac{W_2 - W_1}{W_1} \times 100 \quad (12)$$

where W_1 and W_2 denote the weight of the dry film and the weight of the swollen sample after removing surface moisture and drying, respectively.

2.6. Statistical analysis

Mean values and standard deviations of the analyzed samples were reported. To determine significant differences among the samples, a one-way analysis of variance (ANOVA) was conducted using Tukey's method and a 95% confidence level ($p < 0.05$) with MINITAB 18 software (State College, USA).

3. Results and discussion

3.1. The effect of treatment on PCR composition and lignin recovery

Organosolv lignin extraction from PCR was conducted under the specified treatment conditions, and the composition of untreated and treated PCR is illustrated in Fig. 1. Table 1 presents material and lignin recovery, lignin and xylan removal, and lignin yield of precipitated lignins at different treatment conditions. It is noteworthy that during treatment, a substantial portion of PCR (27.1-51.5 wt.%) was transferred to the liquid phase on the substrate. Similar findings were reported in the literature [35], where variations in ethanol concentration had a negligible impact on solid recovery while increasing the temperature of the organosolv treatment led to a decreas e in solid recovery efficiency.

Fig. 1 illustrates a significant impact of organosolv treatment on the glucan content of the untreated sample, with percentage improvements ranging from 9.3% to 32.9% compared to the initial amount (47.4%). Specifically, under treatment conditions of 180 °C with 50 v/v% ethanol, the solid residues were found to contain 63.0% glucan. This result aligns with the glucan content reported in the solid residue after organosolv treatment of rice straw using 75 v/v% ethanol and 1 wt.% acid at 180 °C [36].

Approximately 39.6-78.4 wt.% xylan and 30.2-55.9 wt.% lignin were transferred to the liquid phase following treatment with 75 v/v% ethanol. However, reducing the ethanol concentration from 75 v/v% to 50 v/v% resulted in the highest mass transfers of xylan and lignin to the liquid phase, accounting for 82.0 wt.% and 59.5 wt.% removal, respectively.

Table 1 reveals that treatment conditions characterized by higher temperatures result in the highest recovery of PCR-lignins. For example, when treated with 75% ethanol at 120 °C, the lignin recovery was 41.7%, but this recovery increased to 73.7% when the treatment temperature was raised to 180 °C. Similar findings have been reported in the literature [25]. The highest lignin yield (43.9 wt.%) was achieved under the conditions of 50 v/v% ethanol and 180 °C (Table 1). The extracted lignins under these treatment conditions exhibited purity levels of 43.7% and 88.3% from the first and second stages of lignin precipitation, respectively.

As indicated in Table 1, treatment at 120 °C with 50% ethanol as the solvent resulted in the transfer of 29.2% of the material mass to the liquid phase. This transferred material contained 72.5 g of total lignin and 72.0 g of xylan per 1 kg of PCR. Increasing the temperature from 120 °C to 180 °C led to the removal of 143.0 g of total lignins and 134.4 g of xylan per 1 kg of PCR. Consequently, the highest percentage of material removal was achieved through organosolv

treatment with 50% ethanol at 180 °C (51.5%). Similarly, Najafi et al., 2021 reported the material removal of 57.8% after organosolv pretreatment of olive leaves at 180 °C with 75% ethanol [37].

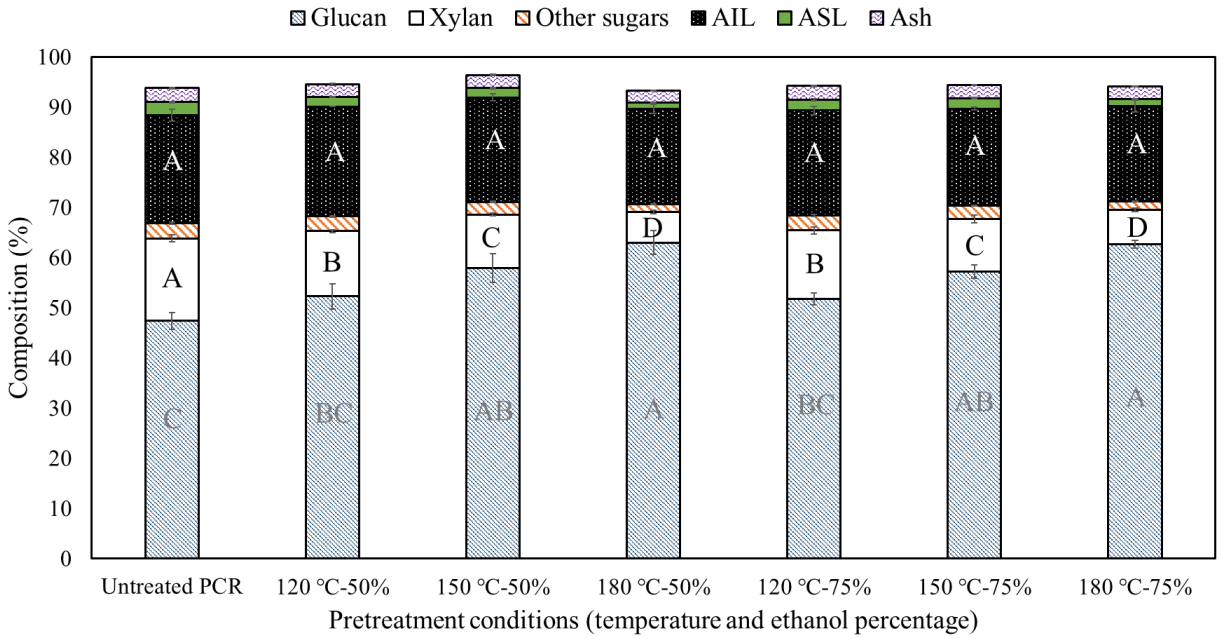

Fig. 1. Percentage of ash, glucan, xylan, other sugars, and lignins (i.e., acid insoluble (AIL), acid soluble (ASL)) in both untreated and treated PCR). Different letters indicate significant differences at $p < 0.05$.

Table 1. Material and lignin recovery, xylan and lignin removal, and lignin yield of precipitated lignins at various treatment conditions.

Treatment conditions		Results of organosolv treatment				
T (°C)	Ethanol (%)	Material recovery (%)	Xylan removal (%)	Lignin recovery (%)	Lignin removal (%)	Lignin yield (%)
120	50	70.8 ± 3.4^{A}	43.7 ± 1.4^{C}	46.1 ± 0.3^{CD}	30.0 ± 2.1^{C}	13.9 ± 0.9^{C}
150	50	63.9 ± 1.7^{A}	58.3 ± 1.1^{B}	59.3 ± 0.3^{B}	39.8 ± 1.4^{B}	23.7 ± 0.7^{B}
180	50	48.5 ± 1.6^{B}	82.0 ± 1.2^{A}	73.5 ± 1.7^{A}	59.5 ± 1.6^{A}	43.9 ± 2.2^{A}
120	75	72.9 ± 2.8^{A}	39.6 ± 3.2^{C}	41.7 ± 0.6^{D}	30.2 ± 1.8^{C}	12.7 ± 0.6^{C}
150	75	66.8 ± 2.2^{A}	57.2 ± 3.4^{B}	53.1 ± 4.4^{BC}	40.8 ± 0.5^{B}	21.8 ± 2.0^{B}
180	75	52.1 ± 1.2^{B}	78.4 ± 0.9^{A}	73.7 ± 1.6^{A}	55.9 ± 2.8^{A}	41.3 ± 1.2^{A}

Data are presented as the mean value ± standard deviation. Different letters in superscript in the same column indicate significant differences at $p < 0.05$.

3.2. Morphology of films, PCR, and PCR-lignins

FE-SEM analysis provided information on the morphology of PCR, PCR-lignins, and fabricated films, the results of which are illustrated in Fig. 2 and Fig. 3. Images for PCR were taken before and after the treatment that produced the highest lignin yield (treatment at 180 °C with 50 v/v% ethanol). Based on the results, untreated PCR had a soft surface and a recalcitrant structure (Fig. 2a). A rough structure appeared, showing either pores or disarray, after being subjected to the condition for the highest lignin yield (Fig. 2b). PCR-lignin particles (Fig. 2c) exhibited approximately spherical geometry.

Neat starch was also analyzed, revealing a smooth and continuous surface (Fig. 3a) due to its high miscibility [38]. Moreover, the absence of pores in the cross-sectional area of films confirms a dense structure, with emerging cracks arising due to film breakage in liquid nitrogen. PCR-lignins at 1 wt.% were well dispersed in the starch matrix, and starch covered filler particles,

310 indicating compatibility between components. Shi & Li [39] stated that the organic solvent
311 (ethanol) added at the film preparation stage contributes to the affinity of lignins and starch.

312 The surface of composite films roughened more with increasing lignins in the matrix (Fig.
313 3e and 3g). Furthermore, the available space for particles declined with an increment in the filler
314 content. PCR-lignin particles, thus, joined to one another and agglomerated owing to the surface
315 energy, hydrogen bonding between these particles, and π-π interactions of lignins [40]. At a lower
316 magnitude, these irregularities were recognized as inhomogeneous parts, expanded for higher
317 proportions of lignins (OPL-11%). Michelin et al. [41] observed the agglomeration of organosolv
318 lignin in carboxymethyl cellulose-based films. Lignin aggregation in butylene adipate-co-
319 terephthalate films due to the self-aggregation of lignin and weak compatibility of filler with the
320 matrix was also reported in the literature [42]. However, it was mentioned that enzymatically
321 modified kraft lignins are well-dispersed in the matrix due to their lower molecular weight
322 fractions [43].

323

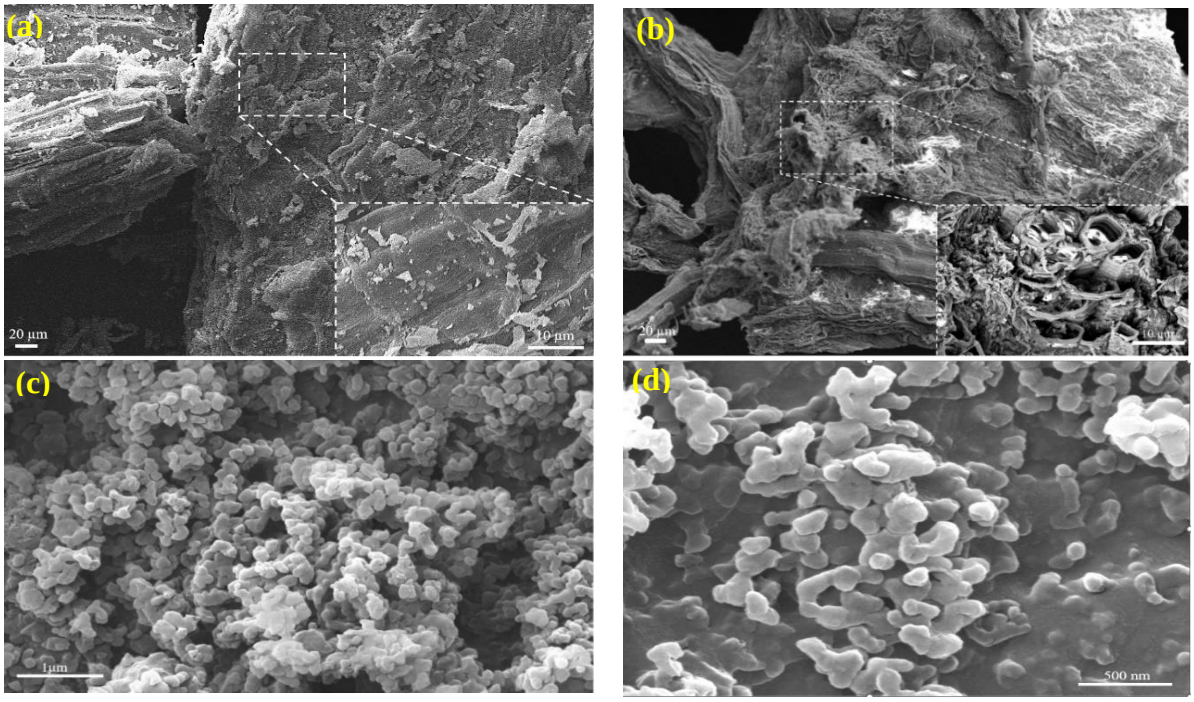

Fig. 2. Morphological images of (a) untreated PCR, (b) treated PCR, (c) PCR-lignins (magnitude 60,000x), and (d) PCR-lignins (magnitude 120,000x).

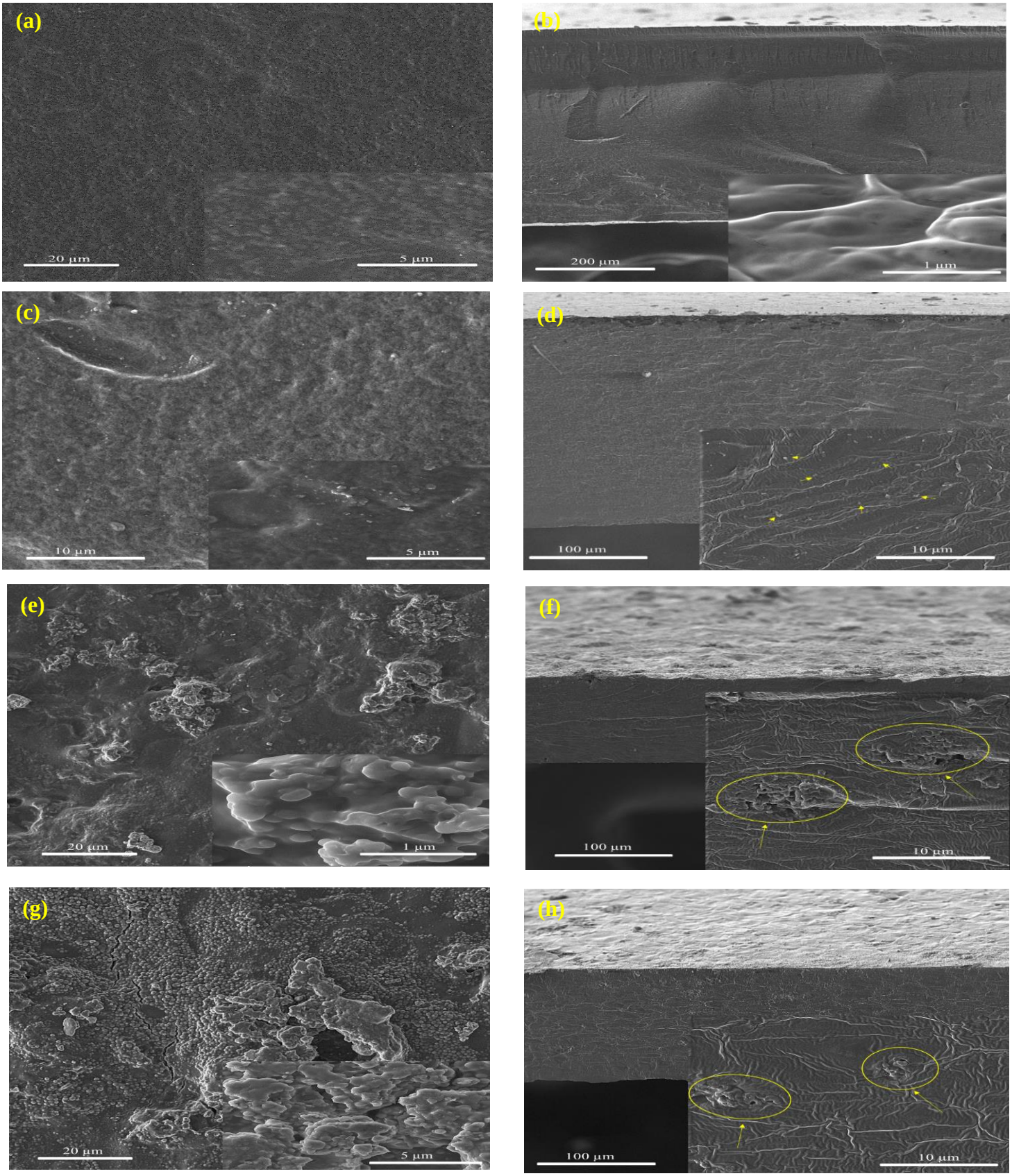

328 **Fig. 3.** Morphological images of the surface of (a) Neat starch, (c) OPL-1%, (e) OPL-7%, and
329 (g) OPL-11%, as well as the cross-section of (b) Neat starch, (d) OPL-1%, (f) OPL-7%, and (h)
330 OPL-11%.

3.3. ATR-FTIR analysis

The spectra obtained from ATR-FTIR analysis, as shown in Fig. 4a, include Neat starch, composite films, and PCR-lignins. The spectrum of the pure starch sample exhibits a peak at 3301 cm^{-1}, indicating the stretching of O-H functionality and the presence of hydroxyl groups. This peak suggests the existence of moisture in the non-crystalline portion of the films, as indicated by the appearance of a peak at 1648 cm^{-1}. Additional peaks at 2922 cm^{-1}, 1150 cm^{-1}, and 924 cm^{-1} are attributed to the stretching of C-H, C-C bonds [44], and C-O stretching in the ether functionality, respectively. The C-O stretching in the C-O-C functional group corresponds to the vibration mode of the α-1,4 glycosidic linkage. Other observed peaks at wavenumbers 852 cm^{-1} and 762 cm^{-1} result from CH_2 deformation vibration and C-C stretching, respectively [45].

Similarly, the spectra of PCR-lignins display peaks at wavenumbers of 3285 cm^{-1}, 2925 cm^{-1}, 2859 cm^{-1}, 1715 cm^{-1}, and 1451 cm^{-1}, corresponding to the stretching of hydroxyl groups, C-H stretching in CH_2, C-H stretching in CH_3, and C-H vibrations of CH_2 and CH_3, respectively. Additional peaks observed at wavenumbers of 1643 cm^{-1} and merged peaks at 1600-1400 cm^{-1} are attributed to C=C skeletal vibrations and indicate the presence of aromatic rings, respectively [46]. Notably, the presence of peaks at 1068 cm^{-1}, 1034 cm^{-1}, and 835 cm^{-1} wavenumbers may indicate the deformation of C-H bonds present in structural units [47].

As anticipated, the spectra of films containing PCR-lignins closely resemble that of the pure starch film. This similarity is due to the fact that the starch matrix remains the primary component in all instances [46]. Fig. 4a illustrates that the addition of PCR-lignins to the starch-based matrix altered the location of the hydroxyl groups, relocating them to lower wavenumbers. This relocation made the peaks more pronounced compared to the control film. This effect is attributed to the interaction between hydroxyl functionalities present in starch and PCR-lignins,

forming hydrogen bonds between the biopolymers. Zhang et al. [4] noted that these interactions enhance the compatibility of the filler and starch, resulting in compact composite samples. Additionally, a new peak at around 1523 cm^{-1} emerged in the biocomposite spectra, attributed to the C=C groups introduced by the added lignins [48].

3.4. XRD analysis

X-ray analysis was conducted to assess the crystalline structure of extracted PCR-lignins and the prepared films, and the resulting diffractogram is depicted in Fig. 4b. In this figure, a broad peak is evident at approximately $2\theta = 17°$, signifying the amorphous nature of PCR-lignins. It is important to note that the characteristics of this peak may exhibit slight variations based on the source of lignins and the separation method employed [49].

The diffractogram of pure starch (Neat starch) unveils a semi-crystalline structure with peaks occurring at approximately $2\theta = 14.7°$, 17°, and 18.5°. These peaks are indicative of V-type crystallinity [50], suggesting the reorganization of amylose with glycerol during the film formation process [51]. Upon the addition of PCR-lignins, these peaks become broader, implying a reduction in the crystallinity of the composite films. Consequently, the biocomposite with a low PCR-lignins content (i.e., OPL-1%) displays a diffractogram resembling that of pure starch. This outcome can be attributed to the amorphous nature of PCR-lignins and aligns with previous research findings that have reported decreased crystallinity in biocomposites due to the presence of residual lignins, as observed in poly(vinyl alcohol)/nanocellulose films [52].

Furthermore, the formation of a more amorphous structure is supported by the ATR-FTIR results. The hydrogen bonds established between the matrix and filler not only enhance the compatibility of the two biopolymers but also impede the development of crystalline structures

within the starch matrix. In essence, these interactions reduce the order of biopolymer molecules and, consequently, the overall crystallinity of the biocomposites [53].

3.5. Thermal stability

TGA analysis was conducted to assess the thermal stabilities of PCR-lignins and the prepared films, with the results presented in Fig. 4c and Fig. 4d. The degradation temperatures and final residues at 700 °C were calculated and are summarized in Table 2.

In the thermograph of PCR-lignins, the extracted lignins exhibited favorable thermal stability, with the highest mass loss occurring in the temperature range of 260-450 °C. This result was expected, as the complex structure of lignins, characterized by aromatic groups, C-C linkages, and ether bonds, has previously been reported to enhance their thermal resistance [46].

For the starch-based composite films, the initial mass loss before 150 °C was attributed to the vaporization of water present in the films, which forms weak bonds with glycerol and starch. Subsequently, between 200 °C and 260 °C, another mass loss occurred due to the degradation of glycerol and the starch matrix, respectively. In the case of PCR-lignins embedded in biocomposites, degradation occurred in the temperature range of 260-390 °C, during which C-C linkages between aromatic and aliphatic moieties were broken. Notably, the highest levels of mass loss for the films were observed at 240-320 °C, and this mass loss was lower for the biocomposites compared to pure starch. This phenomenon can be attributed to the molecular interactions and hydrogen bonds, as indicated by the ATR-FTIR results.

Table 2 reveals that the characteristic temperatures of T_{30}, T_{50}, T_{onset}, and T_{max} were higher for OPL-1% compared to the other samples. Additionally, the DTG (Derivative Thermogravimetry) diagram (Fig. 4d) shows that the peaks for biocomposite samples, except for

OPL-11%, shifted to higher temperatures. For instance, the curve of OPL-1% had a peak at 298 °C (T_{max}), which was the highest T_{max} among all samples. This suggests that the thermal strength of OPL-1% was initially enhanced due to the well-dispersed and thermally stable PCR-lignins in the starch matrix [54]. However, higher concentrations of PCR-lignins (i.e., OPL-7% and OPL-11%) were found to negatively influence thermal stability. This could be attributed to the agglomeration observed at high filler loadings, as evidenced in the FE-SEM results. Filler agglomeration leads to void formation [55], creating pathways for the permeation of volatile degradation products [56]. Consequently, agglomeration reduces the thermal barrier effect of filler particles. Similar findings were reported by Espinoza Acosta et al. [38] for the thermal stability of durum wheat starch and lignin composites.

On the other hand, the mass residue at 700 °C increased with the increment of filler, attributed to the presence of aromatic rings and ether bonds in the structure of lignins [4]. The loading of lignins with thermal stability was higher in the biocomposite samples, leading to an increased char residue in the range of 500-700 °C [39]. Enhanced thermal stability was also observed in protein films with the addition of cone lignins [57]. The increase in T_{max} obtained by Rojas-Lema et al. [57] was approximately 4.5%, slightly higher than that in the present work. However, a significantly higher increase in char residue (63.5%) was evident after the addition of lignins in this study.

417 **Table 2.** TGA data of PCR-lignins, Neat starch, and biocomposites.

	T_{onset} (°C)	T_{max} (°C)	T_5 (°C)	T_{30} (°C)	T_{50} (°C)	Residue (%)
PCR-lignins	240	316	223	331	392	26.6
Neat starch	152	285	137	267	296	2.7
OPL-1%	158	298	140	271	307	3.6
OPL-7%	157	293	142	263	306	5.7
OPL-11%	140	283	146	262	302	7.4

418

419

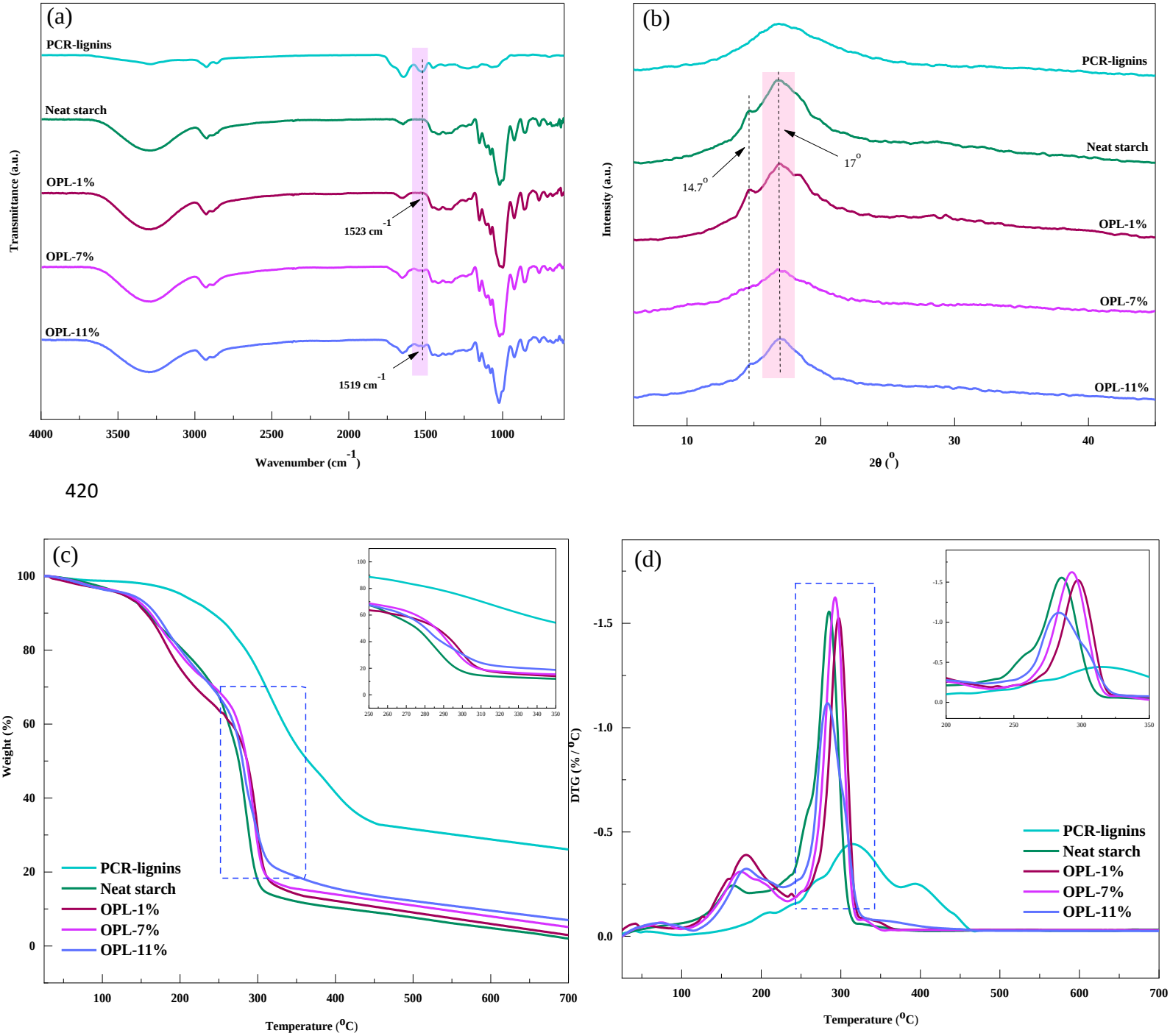

420

421 **Fig. 4.** Characterizations of biocomposite films, PCR-lignins, and Neat starch. a) ATR-FTIR

422 analysis, b) XRD spectra, c) TGA curves, and d) DTG graphs.

423

3.6. Opacity and UV-shielding properties of films

The prepared films need to exhibit acceptable aesthetics and possess UV-blocking properties for potential use in food packaging applications. Consequently, UV-Vis spectrophotometry was employed to measure the opacity and UV transmittance of the fabricated films, and the results are presented in Table 3 and Fig. 5, respectively.

Table 3 demonstrates that the incorporation of PCR-lignins into the starch matrix increased the opacity of the biocomposites. There was a clear positive correlation between the opacity of the films and the amount of filler added, with the highest opacity observed in the sample containing 11 wt.% PCR-lignins, making it the most opaque among all samples. Conversely, Neat starch exhibited the highest transparency, and the biocomposite with 1 wt.% filler content (OPL-1%) was the most transparent. This outcome was expected, as the chromophoric groups present in lignins are known to reduce film transparency. Interestingly, the increased opacity of the films with higher PCR-lignins content could be advantageous for packaging light-sensitive food products. Additionally, lignins' functional groups are associated with UV-blocking properties, which can help reduce the risk of UV radiation-induced food oxidation [31]. This result aligns with previous studies, such as Michelin et al. [41], who reported increased opacity when lignins were incorporated into carboxymethyl cellulose-based films. Furthermore, the introduction of lignins into thermoplastic starch/pectin blend films was found to have a similar effect [58].

In Fig. 5, it is evident that PCR-lignins contributed to higher UV absorbance in the biocomposite films. Notably, OPL-11% exhibited the highest UV absorbance across a broader spectrum, encompassing both UV and visible light. In contrast, Neat starch displayed the lowest absorbance in both the UV and visible light regions. This increase in UV absorbance due to the

inclusion of PCR-lignins supports the UV-blocking properties of the biocomposites, a quality that has been previously explored in the literature [58, 59].

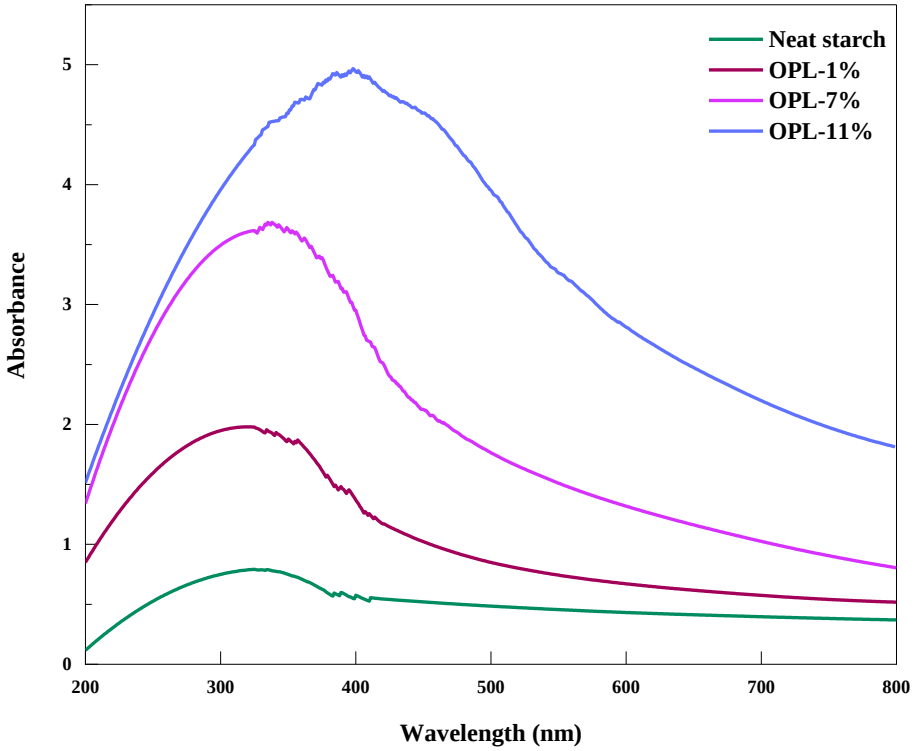

Fig. 5. UV spectra of Neat starch and biocomposite films.

3.7. Oxygen and water barrier properties

The ability of films to prevent the permeation of oxygen and water is crucial for enhancing the shelf life of materials when the film is used in packaging [60]. Therefore, oxygen permeation, water swelling, and water vapor transmission rate (WVTR) were investigated, and the results are presented in Table 3.

The addition of 1 wt.% PCR-lignins reduced oxygen permeation in starch-based films by 87%. However, for composite films with higher filler contents, oxygen permeation increased again. This reduction in oxygen permeation can be attributed to the O-H bonding, as evidenced by ATR-FTIR, which limited the movement of starch chains and decreased gas permeation by reducing the free volume within the matrix [61]. On the other hand, the agglomeration of filler particles observed in the FE-SEM results (Fig. 3e-h) led to the formation of voids in the starch matrix. Consequently, higher oxygen permeation was observed in composites with PCR-lignins content exceeding 1 wt.% compared to Neat starch [62]. Previous literature reported a 65% reduction in oxygen permeation by incorporating lignins into the matrix of starch/pectin blends, which was lower than the results obtained in this study [58].

Incorporating PCR-lignins also reduced WVTR and water swelling in composite films, which can be explained by the inherent hydrophobicity of lignins. Organosolv lignin is fundamentally hydrophobic, reducing the tendency of starch to transmit water. Additionally, while the structure of lignins is generally amphiphilic [41], hydrogen bonds formed between PCR-lignins and starch reduced the availability of hydroxyl groups, limiting their interaction with water. The lowest WVTR and water swelling values were observed for OPL-3%, and an increase in filler content resulted in a marginal increase in WVTR and water swelling due to the presence of agglomerated filler within the matrix. The agglomerated filler may also be present on the surface of biocomposites, leading to defective interactions between the hydroxyl groups of the two components and introducing more free hydroxyl groups to the film. These hydroxyl groups increased the hydrophilicity and water swelling values of the biocomposites [26]. Overall, Neat starch exhibited the highest WVTR and water swelling, and increasing the PCR-lignins content was positively correlated with increased water resistance of the starch-based films. The

lower water vapor permeation has been mentioned to extend the shelf life of fresh fruits, such as grapes [63] and bananas, owing to the decreased transpiration resulting from the reduced difference between the water vapor pressure of fruits and the ambiance [64]. Therefore, the used filler could impart characteristics of prolonged shelf life to biocomposites by reducing WVTR. The impact of lignins on reducing water vapor permeation has also been investigated in previous studies involving various films, including cellulose [16], poly(lactide) [65], and gellan gum [66].

3.8. Antioxidant activity

Antioxidant activity plays a crucial role in preventing food oxidation caused by free radicals and maintaining food quality through the use of active films [58]. The results of the DPPH assay, presented in Table 3, demonstrate a positive impact of PCR-lignins on the antioxidant activity of the films. Neat starch exhibited the lowest antioxidant activity at 8.8%, while the incorporation of 1 wt.% PCR-lignins boosted antioxidant activity to 40.1%, and 67.7% for OPL-7%. This effect was further enhanced with increasing filler content so that antioxidant activity significantly increased, with OPL-11% showing a remarkable 90% improvement. The presence of double bonds and functional groups such as hydroxyl and phenolic groups within the molecule structure of lignins enables them to stabilize free radicals by donating hydrogen and acting as free radical scavengers [58]. Thus, the increase in PCR-lignins loading provided more free radical scavengers, thereby improving antioxidant activity of biocomposites. These results align with findings reported in other studies, which showed that presence of lignins in starch/pectin blend films [58] and carboxymethyl cellulose-lignin enhanced the antioxidant activity of the matrix [67]. Antioxidant activity of 88.74% was evidenced by Worku et al. [68] after adding lignins nanoparticles to polyvinyl alcohol/chitosan films, which was slightly higher, as compared to the achieved value for OPL-11% in this work. Lignins generally exhibited a

similar effect on the antioxidant activity of the films in previous studies, and variations in the obtained values may be attributed to differences in the lignin extraction processes used in various studies and the resulting lignin structures [69].

Table 3. Opacity, oxygen permeability, water swelling, and water vapor transmission rate of films.

Sample	Opacity (A_{600}/mm)	O_2 permeability (10^{-10} $cm^3.cm/cm^2.s.cmHg$)	Water swelling (%)	Water vapor transmission rate (10^{-7} $kg/s.m^2$)	Antioxidant activity (%)
Neat starch	1.0 ± 0.0^{D}	1.5 ± 0.5^{A}	138.3 ± 1.3^{A}	12.0 ± 0.1^{A}	8.8 ± 2.5^{E}
OPL-1%	1.7 ± 0.1^{D}	0.2 ± 0.1^{A}	118.5 ± 6.5^{B}	9.4 ± 0.6^{A}	40.1 ± 1.7^{D}
OPL-3%	4.5 ± 0.2^{C}	0.5 ± 0.2^{A}	69.3 ± 5.4^{D}	9.3 ± 0.0^{A}	42.7 ± 0.5^{CD}
OPL-5%	7.5 ± 0.2^{B}	0.6 ± 0.1^{A}	69.7 ± 7.8^{D}	9.4 ± 0.3^{A}	46.7 ± 1.5^{C}
OPL-7%	8.8 ± 0.7^{B}	0.6 ± 0.2^{A}	88.6 ± 0.3^{C}	9.6 ± 1.1^{A}	67.7 ± 1.3^{B}
OPL-9%	12.2 ± 0.4^{A}	0.7 ± 0.1^{A}	90.8 ± 1.8^{C}	9.7 ± 0.1^{A}	73.9 ± 1.3^{B}
OPL-11%	12.5 ± 0.3^{A}	0.7 ± 0.2^{A}	93.5 ± 3.1^{C}	9.9 ± 0.3	87.7 ± 1.7^{A}

Data are presented as the mean value ± standard deviation. Different letters in superscript in the same column indicate significant differences at $p < 0.05$.

3.9. Mechanical properties

Due to the limited mechanical properties of starch films, PCR-lignins were employed to enhance their strength. Mechanical analysis was conducted to assess the mechanical properties of the prepared films and the impact of introducing the extracted lignins. The tensile test results are displayed in Fig. 6, and detailed information can be found in supplementary Table S2.

It was anticipated that Young's modulus and ultimate tensile strength would exhibit a sustained positive trend due to the interactions and hydrogen bonding between the filler and the matrix. However, Fig. 6 shows that the Young's modulus of the biocomposites increased from approximately 11 MPa to 69 MPa for the OPL-1% loading but decreased to around 65 MPa and 41 MPa with higher filler loadings (OPL-7% and OPL-11%). Notably, OPL-11% exhibited a lower Young's modulus compared to OPL-1% and OPL-7%. The ultimate tensile strength also experienced a slight increase for OPL-1%, but additional PCR-lignins led to a decrease in ultimate tensile strength. Although hydrogen bonding between the two components, as evidenced by ATR-FTIR results, had a positive effect on the mechanical properties of composite films, it was insufficient to form a strong physical cross-linking network within the matrix to achieve ultimate tensile strength higher than the observed values [70].

Furthermore, the high filler loadings and resulting agglomeration led to interfacial defects, reducing interfacial adhesion between the filler and matrix and diminishing the stiffening effect of PCR-lignins. Consequently, this resulted in a decrease in both Young's modulus and ultimate tensile strength for OPL-7% and OPL-11% [71]. The elongation at break of composite films decreased from approximately 60% for Neat Starch to about 40% for OPL-11%, corresponding to the increased PCR-lignins content in the starch-based films. This reduction in elongation at break and increase in Young's modulus due to the presence of PCR-

lignins align with observations reported by Zhang et al. [4]. Freitas et al. [70] also noted a mild increase in tensile strength and a similar trend for the elastic modulus in starch/kraft lignin films. Additionally, Izaguirre et al. [72] observed a decrease in Young's modulus when incorporating organosolv lignin and kraft lignin into chitosan films.

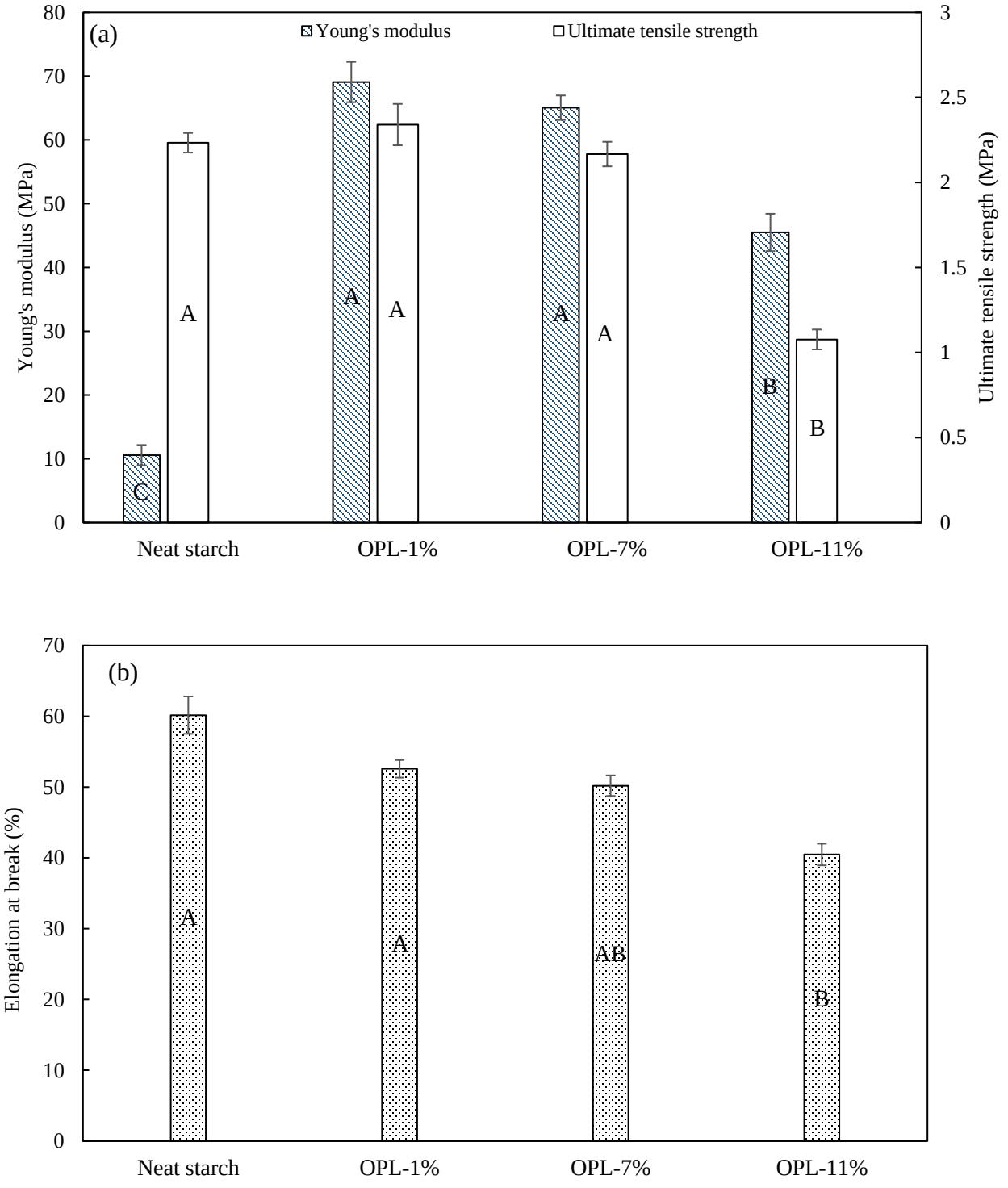

543 **Fig. 6.** Mechanical data of Neat starch and the biocomposites. a) Young's modulus and Ultimate
544 tensile strength. b) Elongation at break. Different letters indicate significant differences at $p <$
545 0.05.

4. Conclusions

Novel biocomposites for biodegradable food packaging were investigated in this study. Organosolv treatment was employed to extract lignins from potato crop residues, resulting in a 59.9% lignin removal. The extracted lignins were used as a filler to produce starch-based films. ATR-FTIR results demonstrated that the incorporation of lignins from potato crop residues into the starch matrix led to a reduction in the hydroxyl stretching frequency. This reduction indicated good compatibility between the added potato crop residues-sourced lignins and starch. XRD analysis confirmed the formation of bonds between these components, and FE-SEM images revealed the effective dispersion of the filler at a low mass ratio. These interactions not only improved thermal and mechanical stability but also enhanced the oxygen and moisture resistance of the composite films. UV absorption results indicated that the chromophoric groups present in the extracted lignins contributed to the development of opaque films with high UV absorbance, making them suitable for protecting sensitive products from UV light. Additionally, interactions between the hydroxyl groups of the filler and starch resulted in a higher Young's modulus for the biocomposites and increased ultimate tensile strength for the starch-based film containing 1 wt.% lignins. Thus, the biocomposite containing 1 wt.% lignins shows promise for applications in food packaging as a renewable alternative to fossil-based plastics.

To extend the applicability of this study on a larger scale, it is imperative to conduct a thorough techno-economic analysis and environmental impact assessment. The current research predominantly operates at a laboratory scale, necessitating an exploration of the feasibility, challenges, and optimization strategies associated with upscaling production to an industrial level. Additionally, the study lacks an examination of the long-term stability and aging characteristics of the biocomposite films. Evaluating how these films retain their properties over

569 extended periods, particularly under real storage conditions, is essential for a comprehensive
570 assessment of their practical viability.

References

[1] M.R. Havstad, Biodegradable plastics, Plastic waste and recycling, Elsevier2020, pp. 97-129. 129. https://doi.org/10.1016/B978-0-12-817880-5.00005-0.

[2] O.V. Okoro, F.D. Faloye, Comparative Assessment of Thermo-Syngas Fermentative and Liquefaction Technologies as Waste Plastics Repurposing Strategies, Agri.Engin. 2(3) (2020) 378-392. https://doi.org/10.3390/agriengineering2030026.

[3] M. Stoica, V.M. Antohi, M.L. Zlati, D. Stoica, The financial impact of replacing plastic packaging by biodegradable biopolymers-A smart solution for the food industry, J. Clean. Prod. 277 (2020) 124013. https://doi.org/10.1016/j.jclepro.2020.124013.

[4] C.-w. Zhang, S.S. Nair, H. Chen, N. Yan, R. Farnood, F.-y. Li, Thermally stable, enhanced water barrier, high strength starch bio-composite reinforced with lignin containing cellulose nanofibrils, Carbohydr. Polym. 230 (2020) 115626. https://doi.org/10.1016/j.carbpol.2019.115626.

[5] Z. Żołek-Tryznowska, J. Holica, Starch films as an environmentally friendly packaging material: Printing performance, J. Clean. Prod. 276 (2020) 124265. https://doi.org/10.1016/j.jclepro.2020.124265.

[6] M. Nasrollahzadeh, M. Sajjadi, S. Iravani, R.S. Varma, Starch, cellulose, pectin, gum, alginate, chitin and chitosan derived (nano) materials for sustainable water treatment: A review, Carbohydr. Polym. 251 (2021) 116986. https://doi.org/10.1016/j.carbpol.2020.116986.

[7] M. Lovera, E. Pérez, A. Laurentin, Digestibility of starches isolated from stem and root tubers of arracacha, cassava, cush–cush yam, potato and taro, Carbohydr. Polym. 176 (2017) 50-55. https://doi.org/10.1016/j.carbpol.2017.08.049.

[8] A. Fonseca-García, E.J. Jiménez-Regalado, R.Y. Aguirre-Loredo, Preparation of a novel biodegradable packaging film based on corn starch-chitosan and poloxamers, Carbohydr. Polym. 251 (2021) 117009. https://doi.org/10.1016/j.carbpol.2020.117009.

[9] S.P. Bangar, S.S. Purewal, M. Trif, S. Maqsood, M. Kumar, V. Manjunatha, A.V. Rusu, Functionality and Applicability of Starch-Based Films: An Eco-Friendly Approach, Foods (Basel, Switzerland) 10(9) (2021). https://doi.org/10.3390/foods10092181.

[10] H. Peidayesh, A. Heydari, K. Mosnáčková, I. Chodák, In situ dual crosslinking strategy to improve the physico-chemical properties of thermoplastic starch, Carbohydr. Polym. 269 (2021) 118250. https://doi.org/10.1016/j.carbpol.2021.118250.

[11] U. Abid, Y.Q. Gill, M.S. Irfan, R. Umer, F. Saeed, Potential applications of polycarbohydrates, lignin, proteins, polyacids, and other renewable materials for the formulation of green elastomers, Int. J. Biol. Macromol. 181 (2021) 1-29. https://doi.org/10.1016/j.ijbiomac.2021.03.057.

[12] L. An, J. Chen, J.W. Heo, J.H. Bae, H. Jeong, Y.S. Kim, Synthesis of lignin-modified cellulose nanocrystals with antioxidant activity via Diels–Alder reaction and its application in carboxymethyl cellulose film, Carbohydr. Polym. 274 (2021) 118651. https://doi.org/10.1016/j.carbpol.2021.118651.

[13] D.M. Oliveira, T.R. Mota, A. Grandis, G.R. de Morais, R.C. de Lucas, M.L. Polizeli, R. Marchiosi, M.S. Buckeridge, O. Ferrarese-Filho, W.D. dos Santos, Lignin plays a key role in determining biomass recalcitrance in forage grasses, Renew. Energ. 147 (2020) 2206-2217. https://doi.org/10.1016/j.renene.2019.10.020.

[14] O.V. Okoro, A. Amenaghawon, D. Podstawczyk, H. Alimoradi, M.R. Khalili, M. Anwar, P.B. Milan, L. Nie, A. Shavandi, Fruit pomace-lignin as a sustainable biopolymer for biomedical applications, J. Clean. Prod. 328 (2021) 129498. https://doi.org/10.1016/j.jclepro.2021.129498.

[15] Z. Ullah, Z. Man, A.S. Khan, N. Muhammad, H. Mahmood, O.B. Ghanem, P. Ahmad, M.-U.H. Shah, M. Raheel, Extraction of valuable chemicals from sustainable rice husk waste using ultrasonic assisted ionic liquids technology, J. Clean. Prod. 220 (2019) 620-629. https://doi.org/10.1016/j.jclepro.2019.02.041.

[16] N.M. Sá, A.L. Mattos, L.M. Silva, E.S. Brito, M.F. Rosa, H.M. Azeredo, From cashew byproducts to biodegradable active materials: Bacterial cellulose-lignin-cellulose nanocrystal nanocomposite films, Int. J. Biol. Macromol. 161 (2020) 1337-1345. https://doi.org/10.1016/j.ijbiomac.2020.07.269.

[17] A. Kumar, B. Biswas, R. Kaur, B.B. Krishna, T. Bhaskar, Hydrothermal oxidative valorisation of lignin into functional chemicals: A review, Bioresour. Technol. 342 (2021) 126016. https://doi.org/10.1016/j.biortech.2021.126016.

[18] R. Roostazadeh, T. Behzad, K. Karimi, Isolation and characterization of lignin-rich particles as byproducts of bioethanol production from wheat straw to reinforce starch composite films, Ind. Crops Prod. 186 (2022) 115175. https://doi.org/10.1016/j.indcrop.2022.115175.

[19] A.S. Khan, Z. Man, M.A. Bustam, C.F. Kait, M.I. Khan, N. Muhammad, A. Nasrullah, Z. Ullah, P. Ahmad, Impact of ball-milling pretreatment on pyrolysis behavior and kinetics of crystalline cellulose, Waste. biomass. valorization. 7 (2016) 571-581. https://doi.org/10.1007/s12649-015-9460-6.

[20] A. Soltaninejad, M. Jazini, K. Karimi, Biorefinery for efficient xanthan gum, ethanol, and biogas production from potato crop residues, Biomass Bioenergy 158 (2022) 106354. https://doi.org/10.1016/j.biombioe.2022.106354.

[21] G. Ginni, S. Kavitha, Y. Kannah, S.K. Bhatia, A. Kumar, M. Rajkumar, G. Kumar, A. Pugazhendhi, N.T.L. Chi, Valorization of agricultural residues: Different biorefinery routes, J. Environ. Chem. Eng. 9(4) (2021) 105435. https://doi.org/10.1016/j.jece.2021.105435.

[22] S. Zhao, M.M. Abu-Omar, Materials based on technical bulk lignin, ACS Sustain. Chem. Eng. 9(4) (2021) 1477-1493. https://doi.org/10.1021/acssuschemeng.0c08882.

[23] J. Iqbal, N. Muhammad, A. Rahim, A.S. Khan, Z. Ullah, G. Gonfa, P. Ahmad, COSMO-RS predictions, hydrogen bond basicity values and experimental evaluation of amino acid-based ionic liquids for lignocellulosic biomass dissolution, J. Mol. Liq. 273 (2019) 215-221. https://doi.org/10.1016/j.molliq.2018.10.044.

[24] M.N. Borand, F. Karaosmanoğlu, Effects of organosolv pretreatment conditions for lignocellulosic biomass in biorefinery applications: a review, J. Renew. Sustain. Energy 10(3) (2018) 033104. https://doi.org/10.1063/1.5025876.

[25] M. Parchami, S. Agnihotri, M.J. Taherzadeh, Aqueous ethanol organosolv process for the valorization of Brewer's spent grain (BSG), Bioresour. Technol. 362 (2022) 127764. https://doi.org/10.1016/j.biortech.2022.127764.

[26] S. Zolfaghari, S.S. Hashemi, K. Karimi, M. Sadeghi, Valorization of cheese whey to eco-friendly food packaging and biomethane via a biorefinery, J. Clean. Prod. 366 (2022) 132870. https://doi.org/10.1016/j.jclepro.2022.132870.

[27] L.-Y. Liu, S.C. Patankar, R.P. Chandra, N. Sathitsuksanoh, J.N. Saddler, S. Renneckar, Valorization of bark using ethanol–water organosolv treatment: Isolation and characterization of crude lignin, ACS Sustain. Chem. Eng. 8(12) (2020) 4745-4754. https://doi.org/10.1021/acssuschemeng.9b06692.

[28] J. Wildschut, A.T. Smit, J.H. Reith, W.J. Huijgen, Ethanol-based organosolv fractionation of wheat straw for the production of lignin and enzymatically digestible cellulose, Bioresour. Technol. 135 (2013) 58-66. https://doi.org/10.1016/j.biortech.2012.10.050.

[29] A. Sluiter, B. Hames, R. Ruiz, C. Scarlata, J. Sluiter, D. Templeton, D. Crocker, Determination of structural carbohydrates and lignin in biomass, Laboratory analytical procedure 1617(1) (2008) 1-16.

[30] ASTM, Standard Test Method for Tensile Properties of Thin Plastic Sheeting, D882-10, Annual Book of American Standard Testing Methods (2010).

[31] E.M. Zadeh, S.F. O'Keefe, Y.-T. Kim, Utilization of lignin in biopolymeric packaging films, ACS omega 3(7) (2018) 7388-7398. https://doi.org/10.1021/acsomega.7b01341.

[32] S. Mao, F. Li, X. Zhou, C. Lu, T. Zhang, Characterization and sustained release study of starch-based films loaded with carvacrol: A promising UV-shielding and bioactive nanocomposite film, LWT 180 (2023) 114719. https://doi.org/10.1016/j.lwt.2023.114719.

[33] D. ASTM, Standard test method for determining gas permeability characteristics of plastic film and sheeting, D1434, West Conshohocken: ASTM International (2003).

[34] S. Astm, Standard Test Methods for Water Vapor Transmission of Materials—ASTM E96-95, ASTM: West Conshohocken, PA, USA (2004).

[35] A. Soltaninejad, M. Jazini, K. Karimi, Sustainable bioconversion of potato peel wastes into ethanol and biogas using organosolv pretreatment, Chemosphere. 291 (2022) 133003. https://doi.org/10.1016/j.chemosphere.2021.133003.

[36] H. Amiri, K. Karimi, H. Zilouei, Organosolv pretreatment of rice straw for efficient acetone, butanol, and ethanol production, Bioresour. Technol. 152 (2014) 450-456. https://doi.org/10.1016/j.biortech.2013.11.038.

[37] E. Najafi, E. Castro, K. Karimi, Biorefining for olive wastes management and efficient bioenergy production, Energy Convers. Manag. 244 (2021) 114467. https://doi.org/10.1016/j.enconman.2021.114467.

[38] J.L. Espinoza Acosta, P.I. Torres Chávez, B. Ramírez-Wong, L.A. Bello-Pérez, A. Vega Ríos, E. Carvajal Millán, M. Plascencia Jatomea, A.I. Ledesma Osuna, Mechanical, thermal, and antioxidant properties of composite films prepared from durum wheat starch and lignin, Starch-Stärke 67(5-6) (2015) 502-511. https://doi.org/10.1002/star.201500009.

[39] R. Shi, B. Li, Synthesis and characterization of cross-linked starch/lignin film, Starch-Stärke 68(11-12) (2016) 1224-1232. https://doi.org/10.1002/star.201500331.

[40] X. Zhang, W. Liu, W. Liu, X. Qiu, High performance PVA/lignin nanocomposite films with excellent water vapor barrier and UV-shielding properties, Int. J. Biol. Macromol. 142 (2020) 551-558. https://doi.org/10.1016/j.ijbiomac.2019.09.129.

[41] M. Michelin, A.M. Marques, L.M. Pastrana, J.A. Teixeira, M.A. Cerqueira, Carboxymethyl cellulose-based films: Effect of organosolv lignin incorporation on physicochemical and antioxidant properties, J. Food Eng. 285 (2020) 110107. https://doi.org/10.1016/j.jfoodeng.2020.110107.

[42] S.-J. Xiong, B. Pang, S.-J. Zhou, M.-K. Li, S. Yang, Y.-Y. Wang, Q. Shi, S.-F. Wang, T.-Q. Yuan, R.-C. Sun, Economically competitive biodegradable PBAT/lignin composites: Effect of lignin methylation and compatibilizer, ACS Sustain. Chem. Eng. 8(13) (2020) 5338-5346. https://doi.org/10.1021/acssuschemeng.0c00789.

[43] S.W.A. Shah, K. Ma, R. Ullah, E.A. Ali, A. Qayum, N. Uddin, D. Zhu, Laccase and dye-decolorizing peroxidase-modified lignin incorporated with keratin-based biodegradable film: An elucidation of structural characterization, antibacterial and antioxidant properties, Food. Chem. (2023) 101035. https://doi.org/10.1016/j.fochx.2023.101035.

[44] A. Pourfarzad, A. Yousefi, K. Ako, Steady/dynamic rheological characterization and FTIR study on wheat starch-sage seed gum blends, Food Hydrocoll. 111 (2021) 106380. https://doi.org/10.1016/j.foodhyd.2020.106380.

[45] J. Xiong, Q. Li, Z. Shi, J. Ye, Interactions between wheat starch and cellulose derivatives in short-term retrogradation: Rheology and FTIR study, Food Res. Int. 100 (2017) 858-863. https://doi.org/10.1016/j.foodres.2017.07.061.

[46] M. Aqlil, A. Moussemba Nzenguet, Y. Essamlali, A. Snik, M. Larzek, M. Zahouily, Graphene oxide filled lignin/starch polymer bionanocomposite: structural, physical, and mechanical studies, J. Agric. Food Chem. 65(48) (2017) 10571-10581. https://doi.org/10.1021/acs.jafc.7b04155.

[47] W. Wang, Y. Liu, Y. Wang, L. Liu, C. Hu, The influence of solvent on the pyrolysis of organosolv lignins extracted from willow, Energy Convers. Manag.: X 13 (2022) 100139. https://doi.org/10.1016/j.ecmx.2021.100139.

[48] S.N. Mousavi, N. Nazarnezhad, G. Asadpour, S.K. Ramamoorthy, A. Zamani, Ultrafine friction grinding of lignin for development of starch biocomposite films, Polymers 13(12) (2021) 2024. https://doi.org/10.3390/polym13122024.

[49] R.A.C. Gomide, A.C.S. de Oliveira, D.A.C. Rodrigues, C.R. de Oliveira, O.B.G. de Assis, M.V. Dias, S.V. Borges, Development and characterization of lignin microparticles for physical and antioxidant enhancement of biodegradable polymers, J. Polym. Environ. 28 (2020) 1326-1334. https://doi.org/10.1007/s10924-020-01685-z.

[50] H. Yang, M. Tang, W. Wu, W. Ding, B. Ding, X. Wang, Study on inhibition effects and mechanism of wheat starch retrogradation by polyols, Food Hydrocoll. 121 (2021) 106996. https://doi.org/10.1016/j.foodhyd.2021.106996.

[51] D. Domene-López, J.J. Delgado-Marín, I. Martin-Gullon, J.C. García-Quesada, M.G. Montalbán, Comparative study on properties of starch films obtained from potato, corn and wheat using 1-ethyl-3-methylimidazolium acetate as plasticizer, Int. J. Biol. Macromol. 135 (2019) 845-854. https://doi.org/10.1016/j.ijbiomac.2019.06.004.

[52] E. Espinosa, I. Bascón-Villegas, A. Rosal, F. Pérez-Rodríguez, G. Chinga-Carrasco, A. Rodríguez, PVA/(ligno) nanocellulose biocomposite films. Effect of residual lignin content on structural, mechanical, barrier and antioxidant properties, Int. J. Biol. Macromol. 141 (2019) 197-206. https://doi.org/10.1016/j.ijbiomac.2019.08.262.

[53] Y. Zhao, J.S. Teixeira, M.M. Gänzle, M.D. Saldaña, Development of antimicrobial films based on cassava starch, chitosan and gallic acid using subcritical water technology, J. Supercrit. Fluids 137 (2018) 101-110. https://doi.org/10.1016/j.supflu.2018.03.010.

[54] D.S. Bajwa, X. Wang, E. Sitz, T. Loll, S. Bhattacharjee, Application of bioethanol derived lignin for improving physico-mechanical properties of thermoset biocomposites, Int. J. Biol. Macromol. 89 (2016) 265-272. https://doi.org/10.1016/j.ijbiomac.2016.04.077.

[55] P. Jagadeesh, M. Puttegowda, S. Mavinkere Rangappa, S. Siengchin, Influence of nanofillers on biodegradable composites: A comprehensive review, Polym. Compos. 42(11) (2021) 5691-5711. https://doi.org/10.1002/pc.26291.

[56] C. Lee, M.M. Pang, S.C. Koay, H.L. Choo, K.Y. Tshai, Talc filled polylactic-acid biobased polymer composites: Tensile, thermal and morphological properties, SN Appl. Sci. 2 (2020) 1-6. https://doi.org/10.1007/s42452-020-2172-y.

[57] S. Rojas-Lema, K. Nilsson, M. Langton, J. Trifol, J. Gomez-Caturla, R. Balart, D. Garcia-Garcia, R. Moriana, The effect of pine cone lignin on mechanical, thermal and barrier properties of faba bean protein films for packaging applications, J. Food Eng. 339 (2023) 111282. https://doi.org/10.1016/j.jfoodeng.2022.111282.

[58] D. de Oliveira Begali, L.F. Ferreira, A.C.S. de Oliveira, S.V. Borges, A.R. de Sena Neto, C.R. de Oliveira, M.I. Yoshida, C.I. Sarantopoulos, Effect of the incorporation of lignin microparticles on the properties of the thermoplastic starch/pectin blend obtained by extrusion, Int. J. Biol. Macromol. 180 (2021) 262-271. https://doi.org/10.1016/j.ijbiomac.2021.03.076.

[59] X. Li, Y. Liu, X. Ren, Transparent and ultra-tough PVA/alkaline lignin films with UV shielding and antibacterial functions, Int. J. Biol. Macromol. 216 (2022) 86-94. https://doi.org/10.1016/j.ijbiomac.2022.06.188.

[60] D.R. Tapia-Blácido, B.C. Maniglia, M.M. Tosi, Transport phenomena in edible films, Polymers for food applications (2018) 149-192. https://doi.org/10.1007/978-3-319-94625-2_7.

[61] V.P. Swapna, V.S. Abhisha, R. Stephen, Polymer/polyhedral oligomeric silsesquioxane nanocomposite membranes for pervaporation, Polymer nanocomposite membranes for pervaporation, Elsevier2020, pp. 201-229. https://doi.org/10.1016/B978-0-12-816785-4.00009-4.

[62] C. Wolf, H. Angellier-Coussy, N. Gontard, F. Doghieri, V. Guillard, How the shape of fillers affects the barrier properties of polymer/non-porous particles nanocomposites: A review, J. Membr. Sci. 556 (2018) 393-418. https://doi.org/10.1016/j.memsci.2018.03.085.

[63] S.P. Bangar, W.S. Whiteside, F. Ozogul, K.D. Dunno, G.A. Cavender, P. Dawson, Development of starch-based films reinforced with cellulosic nanocrystals and essential oil to extend the shelf life of red grapes, Food. Biosci. 47 (2022) 101621. https://doi.org/10.1016/j.fbio.2022.101621.

[64] S. Tanpichai, K. Thongdonson, A. Boonmahitthisud, Enhancement of the mechanical properties and water barrier properties of thermoplastic starch nanocomposite films by chitin nanofibers: Biodegradable coating for extending banana shelf life, J. Mater. Res. Technol. 26 (2023) 5617-5625. https://doi.org/10.1016/j.jmrt.2023.08.244.

[65] S. Shankar, J.-W. Rhim, K. Won, Preparation of poly (lactide)/lignin/silver nanoparticles composite films with UV light barrier and antibacterial properties, Int. J. Biol. Macromol. 107 (2018) 1724-1731. https://doi.org/10.1016/j.ijbiomac.2017.10.038.

[66] B. Rukmanikrishnan, S. Ramalingam, S.K. Rajasekharan, J. Lee, J. Lee, Binary and ternary sustainable composites of gellan gum, hydroxyethyl cellulose and lignin for food packaging applications: Biocompatibility, antioxidant activity, UV and water barrier properties, Int. J. Biol. Macromol. 153 (2020) 55-62. https://doi.org/10.1016/j.ijbiomac.2020.03.016.

[67] M.T. Haqiqi, W. Bankeeree, P. Lotrakul, P. Pattananuwat, H. Punnapayak, R. Ramadhan, T. Kobayashi, R. Amirta, S. Prasongsuk, Antioxidant and UV-blocking properties of a carboxymethyl cellulose–lignin composite film produced from oil palm empty fruit bunch, ACS omega 6(14) (2021) 9653-9666. https://doi.org/10.1021/acsomega.1c00249.

[68] L.A. Worku, M.G. Tadesse, A. Bachheti, D. Pandey, A.K. Chandel, A.W. Ewuntu, R.K. Bachheti, Experimental investigations on PVA/chitosan and PVA/chitin films for active food packaging using Oxytenanthera abyssinica lignin nanoparticles and its UV-shielding, antimicrobial, and antiradical effects, Int. J. Biol. Macromol. 254 (2024) 127644. https://doi.org/10.1016/j.ijbiomac.2023.127644.

[69] X. Pan, J.F. Kadla, K. Ehara, N. Gilkes, J.N. Saddler, Organosolv ethanol lignin from hybrid poplar as a radical scavenger: relationship between lignin structure, extraction conditions, and antioxidant activity, J. Agric. Food Chem. 54(16) (2006) 5806-5813. https://doi.org/10.1021/jf0605392.

[70] A.d.S. de Freitas, J.S. Rodrigues, C.C. Maciel, A.A. Pires, A.P. Lemes, M. Ferreira, V.R. Botaro, Improvements in thermal and mechanical properties of composites based on thermoplastic starch and Kraft Lignin, Int. J. Biol. Macromol. 184 (2021) 863-873. https://doi.org/10.1016/j.ijbiomac.2021.06.153.

[71] Y. Zare, K.Y. Rhee, D. Hui, Influences of nanoparticles aggregation/agglomeration on the interfacial/interphase and tensile properties of nanocomposites, Compos. B: Eng. 122 (2017) 41-46. https://doi.org/10.1016/j.compositesb.2017.04.008.

[72] N. Izaguirre, O. Gordobil, E. Robles, J. Labidi, Enhancement of UV absorbance and mechanical properties of chitosan films by the incorporation of solvolytically fractionated lignins, Int. J. Biol. Macromol. 155 (2020) 447-455. https://doi.org/10.1016/j.ijbiomac.2020.03.162.